Rotational and relative translational control for satellite electromagnetic formation flying in low earth orbit

Li Fan
Tsinghua University, Beijing, China, and
Min Hu and Mingqi Yang
Space Engineering University, Beijing, China

Abstract

Purpose – The purpose of this paper is to develop a theoretical design for the attitude control of electromagnetic formation flying (EMFF) satellites, present a nonlinear controller for the relative translational control of EMFF satellites and propose a novel method for the allocation of electromagnetic dipoles.

Design/methodology/approach – The feedback attitude control law, magnetic unloading algorithm and large angle manoeuvre algorithm are presented. Then, a terminal sliding mode controller for the relative translation control is put forward and the convergence is proved. Finally, the control allocation problem of electromagnetic dipoles is formulated as an optimization issue, and a hybrid particle swarm optimization (PSO) – sequential quadratic programming (SQP) algorithm to optimize the free dipoles. Three numerical simulations are carried out and results are compared.

Findings – The proposed attitude controller is effective for the sun-tracking process of EMFF satellites, and the magnetic unloading algorithm is valid. The formation-keeping scenario simulation demonstrates the effectiveness of the terminal sliding model controller and electromagnetic dipole calculation method.

Practical implications – The proposed method can be applied to solve the attitude and relative translation control problem of EMFF satellites in low earth orbits.

Originality/value – The paper analyses the attitude control problem of EMFF satellites systematically and proposes an innovative way for relative translational control and electromagnetic dipole allocation.

Keywords Sun tracking, Dipole, Electromagnetic formation flying, Large attitude manoeuvre, Magnetic unloading, Terminal sliding mode control

Paper type Research paper

Introduction

Satellite electromagnetic formation flying (EMFF) has attracted the attention of researchers in the last 10 years for its merits of propellant-free and no contamination of optical sensors. The EMFF concept can be realized by equipping formation flying satellites with three orthogonal electromagnetic coils and reaction wheels, and the relative position and attitude of formation flying satellites can be controlled by the magnetic interactions. Moreover, the concept can be implemented in many future missions, such as fractionated spacecraft, astronomical interferometry and robotic assembly (Alvisio, 2015).

Professor Miller's team proposed the EMFF concept; subsequently, studies have been conducted by the Space Systems Laboratory at the Massachusetts Institute of Technology (Kong *et al.*, 2004). These studies investigated the magnetic dipole model, dynamics analysis, controller design and ground simulation issue, which paved the way for future EMFF research. Professor Sedwick's team investigated the resonant induction near-field generation system (RINGS), which is the first demonstration of EMFF in a microgravity environment (Porter *et al.*, 2014). In recent years, a lot of research on EMFF has also been conducted in China, which mainly focuses on the relative equilibrium state of EMFF, dynamics and control of EMFF. Various controllers have been proposed, such as the finite-time controller (Zeng and Hu, 2012), error feedback controller (Cai *et al.*, 2013), adaptive controller (Zhang *et al.*, 2014) and LMI-based controller (Huang *et al.*, 2015).

The electromagnetic force and torque are highly coupled; therefore, the translational control and rotational control should be considered together. The reaction wheels can be used to decouple the electromagnetic forces and torques, especially the earth's magnetic disturbance torque. In previous works that mainly focused on the translational dynamic model and the control of EMFF, a perfect attitude control was assumed. The electrical currents, which generate the electromagnetic field, are produced by the solar panels; thus, the attitude of EMFF satellites should be sun-tracking.

The current issue and full text archive of this journal is available on Emerald Insight at: **www.emeraldinsight.com/1748-8842.htm**

Aircraft Engineering and Aerospace Technology: An International Journal
89/6 (2017) 815–825

[DOI 10.1108/AEAT-01-2016-0007]

This work is supported by the National Natural Science Foundation (NNSF) of China through Grant 61403416.

Received 10 January 2016
Revised 22 March 2016
Accepted 28 March 2016

Aircraft Engineering and Aerospace Technology: An International Journal
Volume 89 · Number 6 · 2017 · 815–825

Previous work has focused on satellite attitude control system using reaction wheels (Ismail *et al.*, 2015), reaction wheel control with low-speed friction compensation and robust controller design (Wu *et al.*, 2015). However, minimal literature has addressed the large angle manoeuvre problem of EMFF satellites. Moreover, according to Newton's third law, the electromagnetic force is an internal force. Therefore, for an EMFF consisting of n satellites, only $3(n-1)$ constraint functions can be given, and the free magnetic moment should be designed to achieve the optimal solution.

This paper focuses on the rotational and relative translational control of the EMFF. First, the attitude dynamics equations, relative translational dynamics equations and electromagnetic dipole models are derived. Second, a feedback control law of attitude control system, magnetic unloading algorithm of the wheels and large angle manoeuvre algorithms are proposed. Third, the terminal sliding mode controller for relative translational motion is designed, and the convergence is proved. Then, the dipole calculation issue as an optimization problem is formulated to minimise the angular momentum build-up. Finally, three scenarios are carried out to validate the proposed controller, namely, the large angle attitude manoeuvring scenario, magnetic unloading of reaction wheels scenario and two satellite formation keeping scenario.

Dynamic models

In this section, four reference coordinate systems are defined. The attitude dynamics equations and relative translational dynamics equations are derived, and the electromagnetic force and torque models are obtained afterwards.

Coordinate systems

To describe the rotational and relative translational motion, four reference coordinate systems, namely, J2000 frame, Hill frame, orbital frame and body frame, are defined, which are shown in Figure 1.

J2000 frame is an inertial reference frame that originates from the Earth centre O_E. Its $O_E X_I$ axis points toward the mean equinox of J2000.0, $O_E Z_I$ axis points toward the mean celestial North Pole of J2000.0, and $O_E Z_I$ axis completes the right-handed system.

Hill frame $Oxyz$ is a relative reference frame. Its origin is attached to the centre of mass of the EMFF, Ox axis is aligned with the radial direction, Oz axis points towards the normal direction of the orbital plane and Oy axis completes the right-handed system (Zeng *et al.*, 2012a, 2012b).

Orbital frame $Ox_o y_o z_o$ originates from the centre of mass of the satellite, Oz_o axis points towards the earth's centre, Oy_o axis is aligned with the minus direction of the normal direction of the orbital plane and Ox_o axis completes the right-handed system.

Figure 1 Four reference coordinate systems of the EMFF

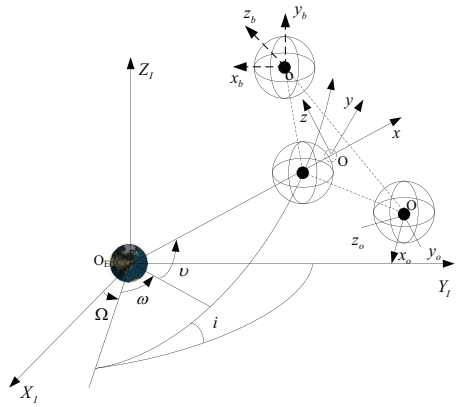

Body frame $Ox_b y_b z_b$ has its origin attached to the centre of mass of the satellite, Ox_b axis is aligned with the longitudinal axis of symmetry and points towards the head of the satellite, Oy_b axis is in the longitudinal plane of symmetry and perpendicular to the Ox_b axis and Oz_b axis completes the right-handed system. If the orbital frame to body frame with 3-2-1 rotation sequence is transformed, then the Euler angles can be defined as yaw(ψ), pitch(θ) and roll(φ) angle (Chak and Varatharajoo, 2015).

Attitude dynamics equations

The spacecraft attitude can be described by the quaternion, which can be defined as follows:

$$\boldsymbol{q} = (q_1 \quad q_2 \quad q_3 \quad q_4)^T \tag{1}$$

where $q_1 = \cos(\phi/2)$, $q_2 = e_x \sin(\phi/2)$, $q_3 = e_y \sin(\phi/2)$ and $q_4 = e_z \sin(\phi/2)$. ϕ denotes the angle of the Euler axis rotation, and $[e_x \; e_y \; e_z]$ is the component of the unit vector of Euler axis. The quaternion should satisfy the following constraint (Wu *et al.*, 2011):

$$q_1^2 + q_2^2 + q_3^2 + q_4^2 = 1 \tag{2}$$

The attitude kinematics based on the quaternion can be rewritten as the linear form:

$$\dot{\boldsymbol{q}} = \frac{1}{2}\begin{bmatrix} 0 & -\omega_{xb} & -\omega_{yb} & -\omega_{zb} \\ \omega_{xb} & 0 & \omega_{zb} & -\omega_{yb} \\ \omega_{yb} & -\omega_{zb} & 0 & \omega_{xb} \\ \omega_{zb} & \omega_{yb} & -\omega_{xb} & 0 \end{bmatrix}\begin{bmatrix} q_1 \\ q_2 \\ q_3 \\ q_4 \end{bmatrix} \tag{3}$$

Supposing that the roll, pitch and yaw angles of the satellite are φ, θ and ψ, respectively, then the transformation matrix from the orbital frame to body frame can be written as:

$$\begin{aligned} \boldsymbol{B}_G &= \begin{bmatrix} 1 & 0 & 0 \\ 0 & \cos\varphi & \sin\varphi \\ 0 & -\sin\varphi & \cos\varphi \end{bmatrix}\begin{bmatrix} \cos\theta & 0 & -\sin\theta \\ 0 & 1 & 0 \\ \sin\theta & 0 & \cos\theta \end{bmatrix}\begin{bmatrix} \cos\psi & \sin\psi & 0 \\ -\sin\psi & \cos\psi & 0 \\ 0 & 0 & 1 \end{bmatrix} \\ &= \begin{bmatrix} \cos\theta\cos\psi & \cos\theta\sin\psi & -\sin\theta \\ \sin\varphi\sin\theta\cos\psi - \cos\varphi\sin\psi & \sin\varphi\sin\theta\sin\psi + \cos\varphi\cos\psi & \sin\varphi\cos\theta \\ \cos\varphi\sin\theta\cos\psi + \sin\varphi\sin\psi & \cos\varphi\sin\theta\sin\psi - \sin\varphi\cos\psi & \cos\varphi\cos\theta \end{bmatrix} \end{aligned} \tag{4}$$

Equation (4) can be approximated as equation (5) when the Euler angles are small.

$$\boldsymbol{B}_G = \begin{bmatrix} 1 & \psi & -\theta \\ -\psi & 1 & \varphi \\ \theta & -\varphi & 1 \end{bmatrix} \tag{5}$$

The angular momentum of the satellite with respect to the body frame is supposed to be $\boldsymbol{H}_I = \boldsymbol{I}_I \cdot \boldsymbol{\omega}_I$, and the corresponding moment is $\boldsymbol{L}_I$. The subscript I denotes that the vectors are in the inertial reference frame. According to the theorem of angular momentum of the rigid body, the following equation is obtained:

$$\frac{d\boldsymbol{H}_I}{dt} = \boldsymbol{L}_I \tag{6}$$

Generally, the rotation equation is established in the body frame. Suppose the transformation matrix from the inertial reference frame to body frame is $\boldsymbol{M}$, then:

$$\begin{gathered} \boldsymbol{I}_B = \boldsymbol{M}\boldsymbol{I}_I\boldsymbol{M}^T, \boldsymbol{\omega}_B = \boldsymbol{M} \cdot \boldsymbol{\omega}_I, \\ \boldsymbol{L}_B = \boldsymbol{M} \cdot \boldsymbol{L}_I \end{gathered} \tag{7}$$

Thus,

$$\boldsymbol{H}_B = \boldsymbol{I}_B \cdot \boldsymbol{\omega}_B = \boldsymbol{M}\boldsymbol{I}_I\boldsymbol{M}^T\boldsymbol{M} \cdot \boldsymbol{\omega}_I = \boldsymbol{M} \cdot \boldsymbol{H}_I \tag{8}$$

According to the theorem of angular momentum, equation (6) can be derived as:

$$\begin{gathered} \frac{d\boldsymbol{H}_I}{dt} = \boldsymbol{L}_I \quad \Rightarrow \quad \frac{d\boldsymbol{H}_B}{dt} = \frac{d\boldsymbol{M}}{dt}\boldsymbol{H}_I \\ + \boldsymbol{M}\frac{d\boldsymbol{H}_I}{dt} = \frac{d\boldsymbol{M}}{dt}\boldsymbol{H}_I + \boldsymbol{L}_B \end{gathered} \tag{9}$$

Thus,

$$\begin{gathered} \frac{d\boldsymbol{M}}{dt} = \frac{\left\{ \begin{bmatrix} 1 & \Delta\psi & -\Delta\theta \\ -\Delta\psi & 1 & \Delta\varphi \\ \Delta\theta & -\Delta\varphi & 1 \end{bmatrix} - I \right\}}{dt} \cdot \\ \boldsymbol{M} = \begin{bmatrix} 0 & \omega_{zb} & -\omega_{yb} \\ -\omega_{zb} & 0 & \omega_{xb} \\ \omega_{yb} & -\omega_{xb} & 0 \end{bmatrix} \cdot \boldsymbol{M} \end{gathered} \tag{10}$$

then:

$$\begin{gathered} \frac{d\boldsymbol{H}_B}{dt} = \begin{bmatrix} 0 & \omega_{zb} & -\omega_{yb} \\ -\omega_{zb} & 0 & \omega_{xb} \\ \omega_{yb} & -\omega_{xb} & 0 \end{bmatrix} \cdot \boldsymbol{M} \cdot \boldsymbol{H}_I \\ + \boldsymbol{L}_B = -\boldsymbol{\omega}_B \times \boldsymbol{H}_B + \boldsymbol{L}_B \end{gathered} \tag{11}$$

Equation (11) is the rotational dynamics equation in the body frame, and the variables are all with respect to the body frame, where:

$$\begin{gathered} \boldsymbol{H}_B = \begin{bmatrix} H_{xb} \\ H_{yb} \\ H_{zb} \end{bmatrix} \boldsymbol{L}_B = \begin{bmatrix} L_{xb} \\ L_{yb} \\ L_{zb} \end{bmatrix} \boldsymbol{\omega}_B = \begin{bmatrix} \omega_{xb} \\ \omega_{yb} \\ \omega_{zb} \end{bmatrix} \begin{bmatrix} H_{xb} \\ H_{yb} \\ H_{zb} \end{bmatrix} \\ \approx \begin{bmatrix} I_{xb} & 0 & 0 \\ 0 & I_{yb} & 0 \\ 0 & 0 & I_{zb} \end{bmatrix} \begin{bmatrix} \omega_{xb} \\ \omega_{yb} \\ \omega_{zb} \end{bmatrix} = \begin{bmatrix} I_{xb}\omega_{xb} \\ I_{yb}\omega_{yb} \\ I_{zb}\omega_{zb} \end{bmatrix} \\ \boldsymbol{\omega}_B \times \boldsymbol{H}_B = \begin{bmatrix} (I_{zb} - I_{yb})\omega_{yb}\omega_{zb} \\ (I_{xb} - I_{zb})\omega_{xb}\omega_{zb} \\ (I_{yb} - I_{xb})\omega_{yb}\omega_{xb} \end{bmatrix} \end{gathered}$$

The rotational dynamics equations in the body frame can be rewritten as follows:

$$\begin{cases} \frac{d}{dt}(I_{xb}\omega_{xb}) + (I_{zb} - I_{yb})\omega_{yb}\omega_{zb} = L_{xb} \\ \frac{d}{dt}(I_{yb}\omega_{yb}) + (I_{xb} - I_{zb})\omega_{xb}\omega_{zb} = L_{yb} \\ \frac{d}{dt}(I_{zb}\omega_{zb}) + (I_{yb} - I_{xb})\omega_{yb}\omega_{xb} = L_{zb} \end{cases} \tag{12}$$

The attitudes of EMFF satellites are assumed to be controlled by three orthogonal reaction wheels, which can be equipped along the axis of the body frame. Suppose the rotational momentum of the reaction wheels are $\boldsymbol{I}_{wx}$, $\boldsymbol{I}_{wy}$ and $\boldsymbol{I}_{wz}$; the angular velocity of reaction wheels with respect to body frame is $\boldsymbol{\omega}_w$; the angular velocity of satellite is $\boldsymbol{\omega}_B$ $\boldsymbol{\omega}_B$; the total rotational momentum of the satellite including the reaction wheels is $\boldsymbol{I}_T$. Thus,

$$\boldsymbol{H}_B = \boldsymbol{I}_T\boldsymbol{\omega}_B + \boldsymbol{I}_w\boldsymbol{\omega}_w \tag{13}$$

Then, the dynamics equation of a rigid satellite is governed as follows:

$$\begin{gathered} \boldsymbol{I}_T\dot{\boldsymbol{\omega}}_B + \boldsymbol{\omega}_B \times (\boldsymbol{I}_T\boldsymbol{\omega}_B) + \boldsymbol{\omega}_B \times (\boldsymbol{I}_w\boldsymbol{\omega}_w) \\ = \boldsymbol{L}_B - \boldsymbol{I}_w\dot{\boldsymbol{\omega}}_w \end{gathered} \tag{14}$$

Relative translational dynamics equation

The relative translational dynamics equation is given by (Liu and Li, 2009):

$$\ddot{\boldsymbol{\rho}} + C(\omega_n)\dot{\boldsymbol{\rho}} + N(\boldsymbol{\rho}, \omega_n, \boldsymbol{r}) + D = \boldsymbol{u}_m \tag{15}$$

where ω_n is the orbital angular velocity of the reference satellite, $\boldsymbol{\rho}(t) = [x(t), y(t), z(t)]^T$ is the relative position of the formation flying satellite to the reference satellite, $\boldsymbol{u}_m$ denotes the relative electromagnetic control acceleration and D denotes the relative disturbances of the satellite and the unmodelled dynamics.

$C(\omega_n) \in R^{3\times3}$ is given by:

$$C(\omega_n) = 2\omega_n \begin{bmatrix} 0 & -1 & 0 \\ 1 & 0 & 0 \\ 0 & 0 & 0 \end{bmatrix} \tag{16}$$

The nonlinear term $N(\cdot) \in R^{3\times3}$ is governed by the following equation:

$$N(\boldsymbol{\rho}, \omega_n, \boldsymbol{r}) = \begin{bmatrix} \mu\left(\dfrac{x + \|\boldsymbol{r}\|}{\|\boldsymbol{r} + \boldsymbol{\rho}\|^3} - \dfrac{1}{\|\boldsymbol{r}\|^2}\right) - \omega_n^2 x \\ \mu\dfrac{y}{\|\boldsymbol{r} + \boldsymbol{\rho}\|^3} - \omega_n^2 y \\ \mu\dfrac{z}{\|\boldsymbol{r} + \boldsymbol{\rho}\|^3} \end{bmatrix} \tag{17}$$

Electromagnetic forces and torques

Schweighart (2005) derived the far-field electromagnetic forces and torques models, which are shown in Figure 2. The far-field model is valid when the ratio of the satellite separation distance to the coil radius is larger than 6.76. In this case, the far-field approximation error is less than 10 per cent.

The electromagnetic force and torque on satellite j by satellite i are expressed as(Huang *et al.*, 2016):

$$\boldsymbol{F}_{ij} = \frac{3\mu_0}{4\pi}\left(-\frac{\boldsymbol{\mu}_i \cdot \boldsymbol{\mu}_j}{r_{ij}^5}\boldsymbol{r}_{ij} - \frac{\boldsymbol{\mu}_i \cdot \boldsymbol{r}_{ij}}{r_{ij}^5}\boldsymbol{\mu}_j - \frac{\boldsymbol{\mu}_j \cdot \boldsymbol{r}_{ij}}{r_{ij}^5}\boldsymbol{\mu}_i + 5\frac{(\boldsymbol{\mu}_i \cdot \boldsymbol{r}_{ij})(\boldsymbol{\mu}_j \cdot \boldsymbol{r}_{ij})}{r_{ij}^7}\boldsymbol{r}_{ij}\right) \tag{18}$$

$$\boldsymbol{T}_{ij} = \frac{\mu_0}{4\pi}\boldsymbol{\mu}_i\left(\frac{3\boldsymbol{r}_{ij}(\boldsymbol{\mu}_j \cdot \boldsymbol{r}_{ij})}{r_{ij}^5} - \frac{\boldsymbol{\mu}_j}{r_{ij}^3}\right) \tag{19}$$

where μ_0 is the permeability of free space and is equal to $4\pi \times 10^{-7}$ H/m. $\boldsymbol{r}_{ij}$ is the relative position vector from satellite i to satellite j, and $\boldsymbol{\mu}_i$ and $\boldsymbol{\mu}_j$ denote the electromagnetic dipoles of satellite i to satellite j, respectively.

We can expand equations (18) and (19) and obtain the following three-dimensional far-field electromagnetic model:

$$\begin{cases} F_{x_A} = \dfrac{3}{4}\dfrac{\mu_0\mu_A\mu_B}{\pi d^4}(2\cos\alpha\cos\beta - \cos(\delta - \chi)\sin\alpha\sin\beta) \\ F_{y_A} = -\dfrac{3}{4}\dfrac{\mu_0\mu_A\mu_B}{\pi d^4}(\cos\alpha\sin\beta\cos\delta + \cos\chi\sin\alpha\cos\beta) \\ F_{z_A} = -\dfrac{3}{4}\dfrac{\mu_0\mu_A\mu_B}{\pi d^4}(\sin\alpha\cos\beta\sin\chi + \cos\alpha\sin\beta\sin\delta) \\ M_{x_A} = -\dfrac{1}{4}\dfrac{\mu_0\mu_A\mu_B}{\pi d^3}\sin\alpha\sin\beta\sin(\delta - \chi) \\ M_{y_A} = \dfrac{1}{4}\dfrac{\mu_0\mu_A\mu_B}{\pi d^3}(\cos\alpha\sin\beta\sin\delta + 2\sin\alpha\cos\beta\sin\chi) \\ M_{z_A} = \dfrac{1}{4}\dfrac{\mu_0\mu_A\mu_B}{\pi d^3}(\cos\alpha\sin\beta\cos\delta + 2\sin\alpha\cos\beta\cos\chi) \end{cases} \tag{20}$$

In equation (20), the electromagnetic forces and torques depend on the product of the magnetic dipole of both satellites and vary as the relative distance and angle change. The electromagnetic force decreases with the relative distance to the fourth power, and electromagnetic torque goes down with the relative distance to the third power. Therefore, the electromagnetic forces and torques are highly nonlinear and coupled.

Figure 2 Far-field electromagnetic model

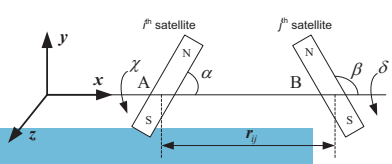

Attitude controller design of EMFF satellites

In this section, the attitude control law is proposed first; then, the unloading algorithm and large-angle manoeuvre algorithm are proposed.

Attitude control law design

Suppose the current quaternion is $\boldsymbol{q}$ and the expected quaternion is $\boldsymbol{q}_c$. Then, the error quaternion $\boldsymbol{q}_e$ is defined as:

$$\boldsymbol{q}_e = \boldsymbol{q}_c^{-1} \otimes \boldsymbol{q} \tag{21}$$

Suppose the current angular velocity is ω and the expected angular velocity is $\boldsymbol{\omega}_c$. Then, the error angular velocity $\boldsymbol{\omega}_e$ is defined as:

$$\boldsymbol{\omega}_e = \boldsymbol{\omega} - \boldsymbol{\omega}_c \tag{22}$$

The attitude dynamics model based on the error quaternion and error angular velocity is governed by:

$$\begin{aligned} &\boldsymbol{I}\dot{\boldsymbol{\omega}}_e + \boldsymbol{I}\dot{\boldsymbol{\omega}}_c + \boldsymbol{\omega}_e \times \boldsymbol{H} + \boldsymbol{\omega}_c \times \boldsymbol{H} = -\boldsymbol{u} + \boldsymbol{M}_d + \boldsymbol{M}_E \\ &\dot{\boldsymbol{q}}_e = \frac{1}{2}\boldsymbol{q}_e \otimes \boldsymbol{\omega}_e \end{aligned} \tag{23}$$

where $\boldsymbol{I}$ is inertial matrix of the whole satellite, $\boldsymbol{H} = \boldsymbol{I\omega} + \boldsymbol{J\Omega}$ is the angular momentum of the whole satellite, $\boldsymbol{u} = \boldsymbol{J\Omega}$ is the control torque of the reaction wheels, $\boldsymbol{M}_d$ is the external disturbance torques and $\boldsymbol{M}_E$ is the disturbance torque caused by the earth's magnetic field. To calculate $\boldsymbol{M}_E$, the magnetic field of the earth can be approximated by a dipole at the centre of the earth (Ahsun *et al.*, 2010).

The nonlinear terms of the nonlinear control system can be offset by using the feedback linearization method. Thus, the feedback control law is proposed as follows:

$$\boldsymbol{u} = -\boldsymbol{I}\dot{\boldsymbol{\omega}}_c - \boldsymbol{\omega}_e \times \boldsymbol{H} - \boldsymbol{\omega}_c \times \boldsymbol{H} + 2\boldsymbol{P}\boldsymbol{q}_{e123} + \boldsymbol{D}\boldsymbol{\omega}_e \tag{24}$$

where $\boldsymbol{P}$ and $\boldsymbol{D}$ represent the constant positive definite gain matrix, which is generally designed as diagonal matrix.

The closed loop of attitude control system after feedback linearization is a typical linear second-order system; hence, the gain matrix of $\boldsymbol{P}$ and $\boldsymbol{D}$ can be determined. The attitude control loop of the satellite consists of dynamics model, sensors, controller and reaction wheel model. The pitch angle control loop is taken as an example. The closed loop diagram is shown in Figure 3.

The models of reaction wheel and gyros can be regarded as transfer functions, and the transfer function of reaction wheels is an inertial element:

Figure 3 Diagram of pitch angle control loop

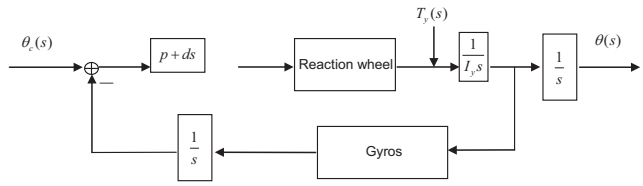

$$W_{wheel} = \frac{1}{\frac{s}{\omega_w} + 1} \tag{25}$$

The transfer function of gyros is an oscillating element:

$$W_{gyro} = \frac{1}{\frac{s^2}{\omega_g^2} + 2\zeta_g \frac{s}{\omega_g} + 1} \tag{26}$$

In Figure 3, the open-loop transfer function of attitude control system consists of the transfer function of dynamics model, transfer function of gyros, transfer function of reaction wheels and PD control law, which can be shown as:

$$W_{open} = \frac{p + ds}{(I_y s^2)\left(\frac{s^2}{\omega_g^2} + 2\zeta_g \frac{s}{\omega_g} + 1\right)\left(\frac{s}{\omega_w} + 1\right)} \tag{27}$$

Then, the closed loop transfer function of attitude control system can be obtained as:

$$W_{close} = \frac{(p + ds)\left(\frac{s^2}{\omega_g} + 2\zeta_g \frac{s}{\omega_g} + 1\right)}{(I_y s^2)\left(\frac{s^2}{\omega_g^2} + 2\zeta_g \frac{s}{\omega_g} + 1\right)\left(\frac{s}{\omega_w} + 1\right) + (p + ds)} \tag{28}$$

The closed loop transfer function model of external disturbance torque $T_y(S)$ to the output of attitude $\theta(S)$ is:

$$W_{disturb} = \frac{\left(\frac{s^2}{\omega_g^2} + 2\zeta_g \frac{s}{\omega_g} + 1\right)\left(\frac{s}{\omega_w} + 1\right)}{(I_y s^2)\left(\frac{s^2}{\omega_g^2} + 2\zeta_g \frac{s}{\omega_g} + 1\right)\left(\frac{s}{\omega_w} + 1\right) + (p + ds)} \tag{29}$$

Then, we can obtain the simplified relationship of input instruction θ_c and external disturbance T_y to the output θ:

$$\theta = W_{close}\theta_c + W_{disturb}T_y \approx \frac{1}{\frac{s^2}{p/I_y} + (d/p)s + 1}\theta_c + \frac{1/p}{\frac{s^2}{p/I_y} + (d/p)s + 1}T_y \tag{30}$$

As shown in equation (30), increasing p can restrain the influence of the disturbances on the attitudes. By contrast, increasing p enlarges the gains of high band, which goes against the stability of flexibility vibration. Therefore, the parameter p should be designed properly. For example, if the attitude tracking error caused by the external disturbances needs to be limited to 0.02°, then $p = 6$ can be chosen. If $I_y = 210$ kgm^2, then $d = 2 \times 0.707 \times \sqrt{Jp} = 50.2$ can be obtained. The Bode diagram of the system is shown in Figure 4.

As Figure 4 shows, the cut-off frequency of system is 0.3 rad/s and the phase margin is larger than 60°.

Figure 4 Bode diagram of open loop of pitch angle

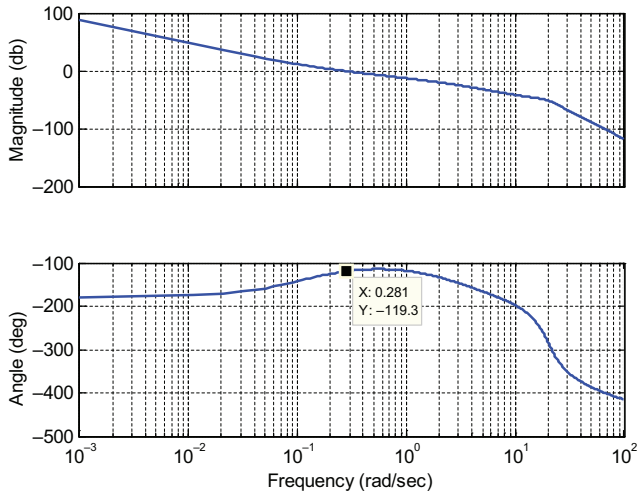

Unloading algorithm design

Magnetic torque is generated by the interaction of the magnetic dipole of the satellite and the earth's magnetic field. Using magnetorquers to unload the reaction wheels is effective for the small satellites in low earth orbit. The redundant momentum of reaction wheels is assumed to be $\Delta \boldsymbol{H}$, and the magnetic momentum can be generated as:

$$\boldsymbol{M} = -\frac{K}{|B|^2}\boldsymbol{B} \times \Delta \boldsymbol{H} \tag{31}$$

where K is the gain coefficient, and the magnetic torque is:

$$\boldsymbol{T} = \boldsymbol{M} \times \boldsymbol{B} = \left(-\frac{K}{|B|^2}\boldsymbol{B} \times \Delta \boldsymbol{H}\right) \times \boldsymbol{B} = -\frac{K}{|B|^2}\{(\boldsymbol{B} \cdot \boldsymbol{B})\Delta \boldsymbol{H} - (\boldsymbol{B} \cdot \Delta \boldsymbol{H})\boldsymbol{B}\} \tag{32}$$

If $\boldsymbol{B}$ is perpendicular to $\Delta \boldsymbol{H}$, then:

$$\boldsymbol{T} = -K\Delta \boldsymbol{H}(K > 0) \tag{33}$$

If $\boldsymbol{B}$ is not perpendicular to $\Delta \boldsymbol{H}$, $\boldsymbol{B}$ can be decomposed into two components. One is situated along the direction of $\Delta \boldsymbol{H}$ called $\boldsymbol{B}_{\Delta H}$, and the other is perpendicular to $\Delta \boldsymbol{H}$ called $\boldsymbol{B}_N$. Then, the torque that contributes to the unloading can be written as:

$$\boldsymbol{T}_1 = -\frac{K}{|B|^2}\{|B|^2 - |B_{\Delta H}|^2\}\Delta \boldsymbol{H} \tag{34}$$

The torque that is not good for unloading can be expressed as:

$$\boldsymbol{T}_2 = \frac{K}{|B|^2}(\boldsymbol{B} \cdot \Delta \boldsymbol{H})\boldsymbol{B}_N \tag{35}$$

Equation (35) shows that, if the angle between $\boldsymbol{B}$ and $\Delta \boldsymbol{H}$ is too small, then it is not suitable for magnetic unloading. Magnetic unloading is generally executed when $|\boldsymbol{b} \cdot \Delta \boldsymbol{H}| < 0.707$, where $\boldsymbol{b}$ and $\Delta \boldsymbol{H}$ are the unit vectors of $\boldsymbol{B}$ and $\Delta \boldsymbol{H}$, respectively. Therefore, the following condition for magnetic unloading can be obtained:

$$45° \angle (\boldsymbol{B}, \Delta\boldsymbol{H}) < 135° \tag{36}$$

If the proportional feedback control law is adopted for momentum unloading, the observed velocity of gyros is $\boldsymbol{\omega}_b$ and the rotational velocity of reaction wheels is $\boldsymbol{\omega}_w$. Thus, the overall angular momentum can be expressed by:

$$\boldsymbol{H} = \boldsymbol{I} \cdot \boldsymbol{\omega}_b + \boldsymbol{I}_w \cdot \boldsymbol{\omega}_w \tag{37}$$

The orbital angular velocity is $\boldsymbol{\omega}_0$, and the nominal angular momentum can be written as:

$$\boldsymbol{H}_0 = \boldsymbol{I} \cdot \boldsymbol{\omega}_0{}^T \tag{38}$$

Therefore, the redundant angular momentum can be expressed as:

$$\Delta\boldsymbol{H} = \boldsymbol{H} - \boldsymbol{H}_0 \approx \boldsymbol{I}_w \cdot \boldsymbol{\omega}_w \tag{39}$$

We can get the magnetic unloading instruction by using proportional feedback control law:

$$\boldsymbol{T} = -K\Delta\boldsymbol{H} \tag{40}$$

Recall that $\boldsymbol{T} = \boldsymbol{M} \times \boldsymbol{B}$; therefore:

$$\boldsymbol{B} \times \boldsymbol{T} = \boldsymbol{B} \times (\boldsymbol{M} \times \boldsymbol{B}) = \boldsymbol{M}(\boldsymbol{B} \cdot \boldsymbol{B}) - \boldsymbol{B}(\boldsymbol{B} \cdot \boldsymbol{M}) \tag{41}$$

If $\boldsymbol{M}$ is parallel to $\boldsymbol{B}$, then the torque cannot be generated, that is, $\boldsymbol{B} \cdot \boldsymbol{M} = 0$. Thus, the following equation can be obtained:

$$\boldsymbol{M} = \boldsymbol{B} \times \boldsymbol{T}/\boldsymbol{B}^2 \tag{42}$$

The unloading magnetic torque is governed by:

$$\begin{aligned} \boldsymbol{T}_{unloading} &= \boldsymbol{M} \times \boldsymbol{B} = \left(-\frac{K}{|B|^2}\boldsymbol{B} \times \Delta\boldsymbol{H}\right) \times \boldsymbol{B} \\ &= -\frac{K}{|B|^2}\{(\boldsymbol{B} \cdot \boldsymbol{B})\Delta\boldsymbol{H} - (\boldsymbol{B} \cdot \Delta\boldsymbol{H})\boldsymbol{B}\} \end{aligned} \tag{43}$$

If $\boldsymbol{B}$ is perpendicular to $\Delta\boldsymbol{H}$, then:

$$\boldsymbol{T}_{unloading} = -K\Delta\boldsymbol{H}(K > 0) \tag{44}$$

Large-angle manoeuvre algorithm design

Orienting the attitudes of EMFF satellites to track the sun to generate enough currents by using solar panels is the best procedure. The typical procedure is to manoeuvre the attitude from three-axis stabilized to sun-tracking. The reaction wheels are used to control the attitude; thus, the maximum torque and the maximum rotation speed limitation cause new issues for large angle manoeuvring. The time optimal manoeuvre algorithm can be designed under the constraints of the maximum torque and rotation speed of the reaction wheels based on the Euler rotation theorem. Moreover, the tracking control can be realized by using the error quaternion and feedback control law of angular speed.

Suppose the nominal attitude before manoeuvring is $\boldsymbol{q}(t_0)$; then, the nominal angular velocity is $\boldsymbol{\omega}(t_0) = [0\ 0\ 0]^T$, the attitude after manoeuvring is $\boldsymbol{q}(t_f)$ and the angular velocity after manoeuvring is $\boldsymbol{\omega}(t_f) = [0\ 0\ 0]^T$. Based on the Euler theorem, the attitude manoeuvring from $\boldsymbol{q}(t_0)$ to $\boldsymbol{q}(t_f)$ can be realized by rotating the instantaneous Euler axis with angle θ, and the manoeuvring path is the shortest. To satisfy the constraint of the maximum torque and rotational speed limitation, the manoeuvring path can be scheduled as:

$$\boldsymbol{L}_c = -\boldsymbol{I}_w\dot{\boldsymbol{\omega}}_w = \boldsymbol{I}_T\dot{\boldsymbol{\omega}}_B + \boldsymbol{\omega}_B \times \boldsymbol{H} - \boldsymbol{L}_B \approx \boldsymbol{I}_T\ddot{\theta}\bar{r} \tag{45}$$

Suppose the maximum output torque of reaction wheels is L_{cmax}, then the maximum angular acceleration around the Euler axis is governed by:

$$\ddot{\theta}_{\max} = \frac{L_{cmax}}{\max(\boldsymbol{I}_T \cdot \bar{r})} \tag{46}$$

To accomplish the attitude manoeuvring as quickly as possible, the manoeuvring path can be scheduled as follows:

$$\dot{\omega}_c(t) = \ddot{\theta}(t)\bar{r}\ \ \omega_c(t) = \dot{\theta}(t)\bar{r}\ \ \boldsymbol{q}_c(t) = \left[\sin\left(\frac{\theta(t)}{2}\right)\bar{r}^T\ \ \cos\left(\frac{\theta(t)}{2}\right)\right]^T \tag{47}$$

To satisfy the constraints of the saturation of reaction wheels, the manoeuvring process should follow the variation law as shown in Figure 5.

As seen in Figure 5, t_1 and t_f are calculated to determine the attitude manoeuvring path. The angular momentum is conserved by ignoring the disturbances during manoeuvring. Therefore:

$$\ddot{\theta}_{\max}t_1^2 + \ddot{\theta}_{\max}t_1(t_f - 2t_1) = \theta_f \Rightarrow t_1 = \frac{1}{2}\left(t_f - \sqrt{t_f^2 - \frac{4\theta_f}{\ddot{\theta}_{\max}}}\right) \tag{48}$$

To ensure that the reaction wheels are not saturated during manoeuvring, manoeuvring time t_f should be determined. Suppose the maximum angular velocity is $\dot{\theta}_{\max}$, then:

$$t_1 = \dot{\theta}_{\max}/\ddot{\theta}_{\max} \tag{49}$$

$$t_f = t_1 + \theta_f/\dot{\theta}_{\max} \tag{50}$$

The t_1 and t_2 calculation flow is illustrated in Figure 6.

The calculation equation of $\boldsymbol{\omega}_{wt}$ can be derived based on the momentum conservation law:

$$\boldsymbol{I}_w\boldsymbol{\omega}_{wt} + \boldsymbol{I}_T\boldsymbol{\omega}_{Bt} = \boldsymbol{I}_w\boldsymbol{\omega}_{w0} + \boldsymbol{I}_T\boldsymbol{\omega}_{B0} \Rightarrow \boldsymbol{\omega}_{wt} \approx -\boldsymbol{I}_w^{-1}\boldsymbol{I}_T\dot{\theta}_i\bar{r} + \boldsymbol{M}(\theta_i)\boldsymbol{\omega}_{w0} \tag{51}$$

Then, the control law can be described as follows:

$$\boldsymbol{L}_c = \boldsymbol{I}_T\dot{\boldsymbol{\omega}}_c + \boldsymbol{\omega} \times \boldsymbol{H} + K_d\boldsymbol{\omega}_e + K_p\boldsymbol{q}_{123} \tag{52}$$

Figure 5 Time variation curves of angular acceleration

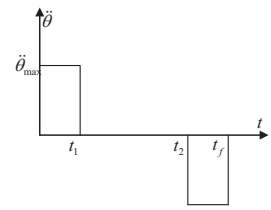

Figure 6 Attitude manoeuvring scheduling flow

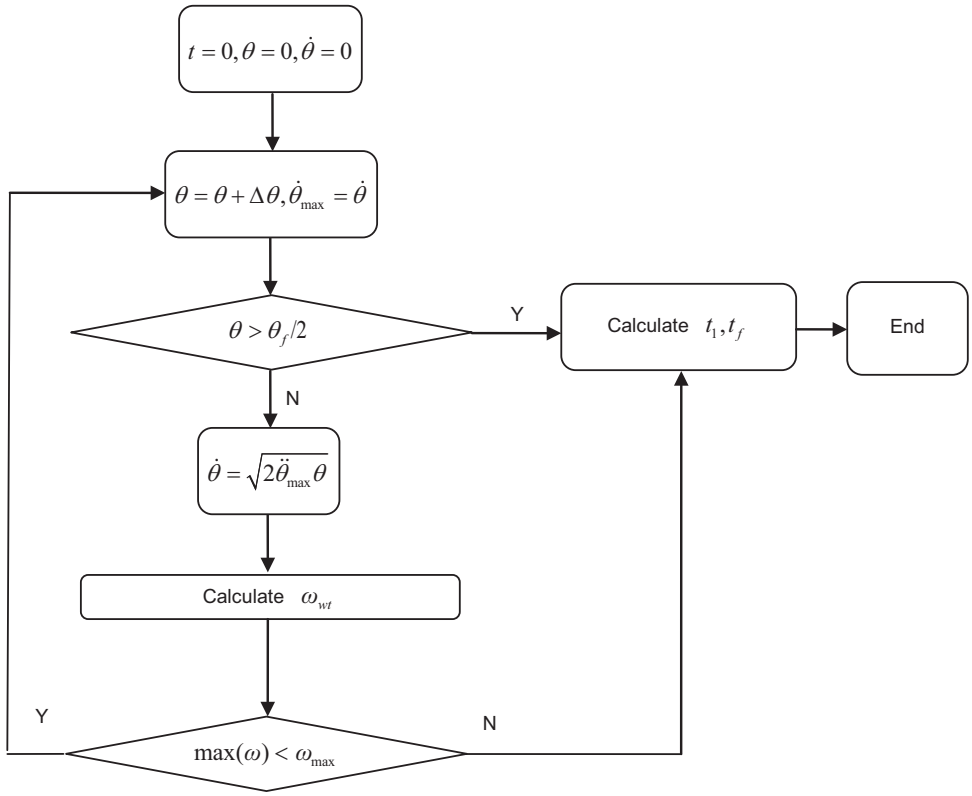

Translational controller design of EMFF satellites

In this section, a terminal sliding mode controller is put forward to control the trajectory tracking errors converge to zero. The trajectory tracking errors are defined as:

$$\boldsymbol{e}=\boldsymbol{\rho}-\boldsymbol{\rho}_d,\quad \dot{\boldsymbol{e}}=\dot{\boldsymbol{\rho}}-\dot{\boldsymbol{\rho}}_d \tag{53}$$

where $\boldsymbol{\rho}_d$, and $\boldsymbol{\rho}_d \in R^3$ are the desired relative position and velocity vectors, respectively.

The terminal sliding mode controller is designed as follows:

$$\boldsymbol{u}_2=C(\omega_n)\dot{\boldsymbol{\rho}}+N(\boldsymbol{\rho},\omega_n,\boldsymbol{r})+\ddot{\boldsymbol{\rho}}_d-\beta\gamma|\boldsymbol{e}|^{\gamma-1}\dot{\boldsymbol{e}}-\boldsymbol{k}sat(S/\phi) \tag{54}$$

where $\alpha, \beta > 0$, $k_i > 0$, $i = 1, 2, 3$, and $0 < \gamma < 1$.

The switch planes can be described as:

$$\boldsymbol{S}_2=\dot{\boldsymbol{e}}+\beta|\boldsymbol{e}|^{\gamma}\,\mathrm{sgn}(\boldsymbol{e}) \tag{55}$$

Theorem. The controller equation (54) can guarantee that the relative translational system given by equation (15) is globally asymptotically stable.

Proof: Define the candidate Lyapunov function as follows:

$$V=\frac{1}{2}\boldsymbol{S}^T\boldsymbol{S} \tag{56}$$

Obviously, equation (56) is positive definite. Differentiating equation (56) with respect to time yields:

$$\begin{aligned}\dot{V}&=S^T\dot{S}=S^T(\ddot{e}+\beta\gamma|\boldsymbol{e}|^{\gamma-1}\dot{e})\\&=S^T(\boldsymbol{u}_m-C(\omega_n)\dot{\boldsymbol{\rho}}-N(\boldsymbol{\rho},\omega_n,\boldsymbol{r})-D-\ddot{\rho}_d+\beta\gamma|\boldsymbol{e}|^{\gamma-1}\dot{e})\\&=S^T[-D-\boldsymbol{k}\,\mathrm{sgn}(\boldsymbol{S})]\end{aligned} \tag{57}$$

Suppose that $|D_i| \le F_i$, and $i = 1, 2, 3$, where F_i is a positive constant; then, setting $k_i > F_i$ yields:

$$\dot{V}\le\sum_{i=1}^{3}(|s_i|F_i-k_i|s_i|)=-\sum_{i=1}^{3}|s_i|(k_i-F_i)\le 0 \tag{58}$$

Therefore, $\dot{V}$ is negative definite. The sliding mode surface can converge to zero. Once $\boldsymbol{S} = 0$, the system can be rewritten as $\dot{\boldsymbol{e}} = -\beta|\boldsymbol{e}|^{\gamma}\,\mathrm{sgn}(\boldsymbol{e})$, and the system state will reach zero in finite time (Yu *et al.*, 1999). Therefore, the system is globally asymptotically stable.

Remark. To eliminate chattering, a saturation function is adopted to replace the signum function of equation (54) with a continuous saturation one (Ding *et al.*, 2007):

$$fsat(S/\phi)=\begin{cases}|S|^{\tau}\,\mathrm{sgn}(S)/\phi^{\tau} & |S|\le\phi\\ \mathrm{sgn}(S) & |S|>\phi\end{cases} \tag{59}$$

where ϕ is the width of the boundary layer and $0 < \tau < 1$. Equation (54) can be rewritten as:

$$\boldsymbol{u}_m=C(\omega_n)\dot{\boldsymbol{\rho}}+N(\boldsymbol{\rho},\omega_n,\boldsymbol{r})+\ddot{\boldsymbol{\rho}}_d-\beta\gamma|\boldsymbol{e}|^{\gamma-1}\dot{\boldsymbol{e}}-\boldsymbol{k}sat(S/\phi) \tag{60}$$

Control allocation of magnetic dipole

According to Newton's third law, the controller equation (60) represents $3(n-1)$ scalar equations for n satellite formations. Therefore, the system is an under-constrained one. Infinite solutions can be obtained.

One way of calculating the magnetic dipole is to fix some dipoles of the EMFF satellites. Consequently, the other dipoles can be calculated by using the following equations:

$$\boldsymbol{F}_{ij} = -\frac{3\mu_0}{4\pi}\cdot\frac{1}{r_{ij}^5}\left[\boldsymbol{r}_{ij}\cdot\boldsymbol{\mu}_j^T + \boldsymbol{\mu}_j\cdot\boldsymbol{r}_{ij}^T + \boldsymbol{\mu}_j^T\cdot\boldsymbol{r}_{ij}\left(I - 5\frac{\boldsymbol{r}_{ij}\cdot\boldsymbol{r}_{ij}^T}{\boldsymbol{r}_{ij}^T\cdot\boldsymbol{r}_{ij}}\right)\right]\boldsymbol{\mu}_i \tag{61}$$

The other way is to formulate the dipole calculation issue as an optimization problem. The optimization goal is to minimise the torques of the reaction wheels and the disturbance torques caused by the earth's magnetic field, which can be expressed as:

$$\mu = \arg\ \min \sum_{i=0}^{N-1}(M_T + M_E) \tag{62}$$

A hybrid PSO-SQP algorithm is proposed to optimize the free dipole. The PSO algorithm is one of the evolutionary computation techniques introduced by Kennedy and Eberhart (1995). The SQP is a nonlinear programming method, which is highly suitable for the nonlinear constraint programming issue (Wilson, 1963). The approach utilizes the PSO to find the initial guess value for the SQP. The SQP technique is used to reduce computation time and to improve convergence performance. A linear decay rule is used to adapt the inertia weight, and the SQP technique is utilized when the convergent value satisfies the predefined threshold.

Simulation and results

This section presents three scenarios to validate the proposed controller. Scenario 1 reports the results of large-angle manoeuvring algorithms for the attitude control of EMFF satellites. Scenario 2 reports the results of magnetic unloading algorithm during the sun-tracking process. Scenario 3 reports the results of terminal sliding mode controller for the formation-keeping process and the electromagnetic dipole allocation algorithms.

Scenario 1. Large-angle manoeuvre for EMFF satellites

The reference orbit is assumed to be sun-synchronous and the orbital altitude is 500 km. The reference orbit parameters are $\{a = 6878137\ \text{m}, e = 0, I = 97.4°, \Omega = 0°, \omega = 0°, M = 0°\}$. The satellite is three-axis stabilized at first, and the target attitude of the EMFF satellite should manoeuvre to track the sun. The perturbations of the earth oblateness, atmospheric drag, solar radiation and third-body of the sun and moon are considered in the simulation. A thirteenth-order EGM96 model is adopted for the earth's gravity field, and the atmospheric density model adopts that of Harris-Priester. The eighth-order Runge-Kuta algorithm is used for the numerical integration. Cr is 1, Cd is 2.2 and the area to mass ratio is 0.01. The moments of inertia matrix are $I_{xx} = 220\ \text{kgm}^2$, $I_{yy} = 210\ \text{kgm}^2$ and $I_{zz} = 57\ \text{kgm}^2$, and the moments of reaction wheels are [0.0095, 0.0095, 0.0095] kgm^2. The limitation of the reaction wheel torques is 0.06 Nm, and the maximum magnetic moment is 50 Am^2. The gain matrix P is [6 6 3], and D is [50 50 18.5]. The simulation epoch is 2016-1-1 12:00:00.00 UTC, and the simulation step is 0.25 s. Three orbits are simulated.

Figure 7 shows the time histories of Euler angle, and Figure 8 shows the time histories of angular velocity.

As shown in Figures 7 and 8, the Euler angles φ, θ and ψ vary periodically during the sun-tracking process. Moreover, once the attitudes have pointed to the sun, the angular velocities are almost stable.

Scenario 2. Magnetic unloading of reaction wheels

The section will prove the effectiveness of the magnetic unloading algorithm during the sun-tracking process. The simulation parameters are the same as those described in Scenario 1.

Figure 9 shows the reaction wheel speeds without magnetic unloading and Figure 10 shows the reaction wheel speeds when magnetic unloading is considered.

Figure 7 Time histories of Euler angle

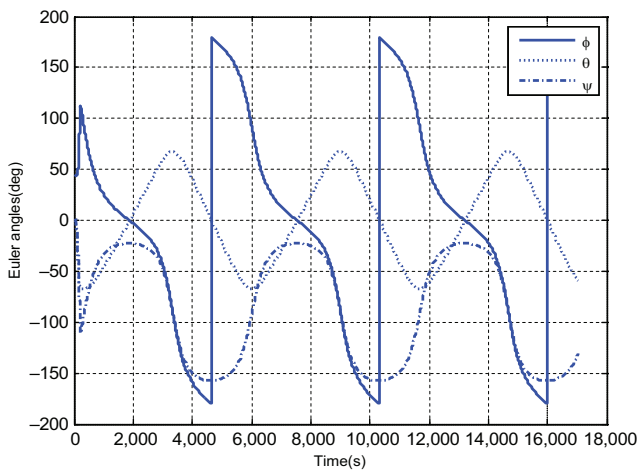

Figure 8 Time histories of angular velocity

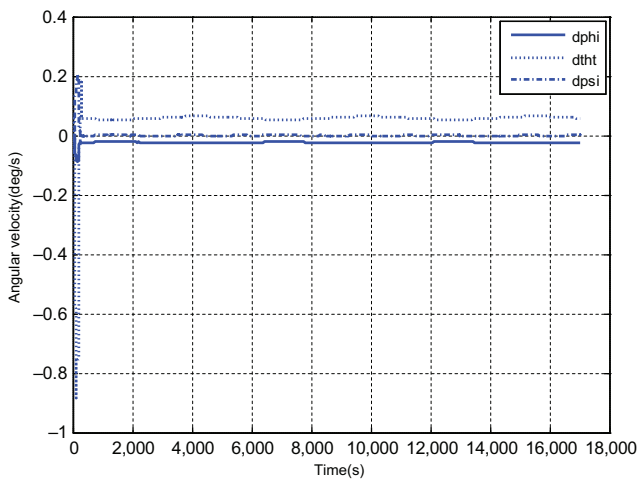

Figure 9 Reaction wheel speed without magnetic unloading control

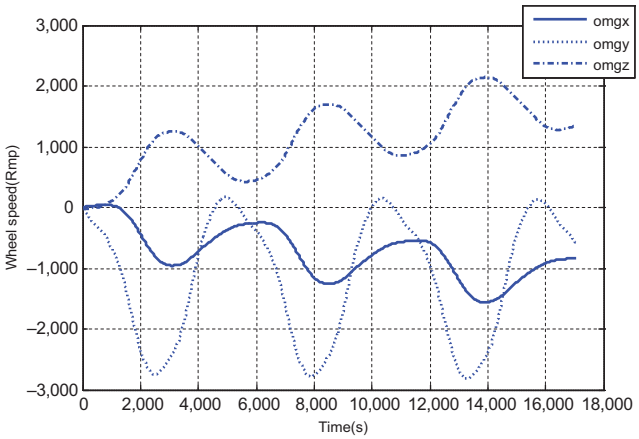

Figure 10 Reaction wheel speed with magnetic unloading control

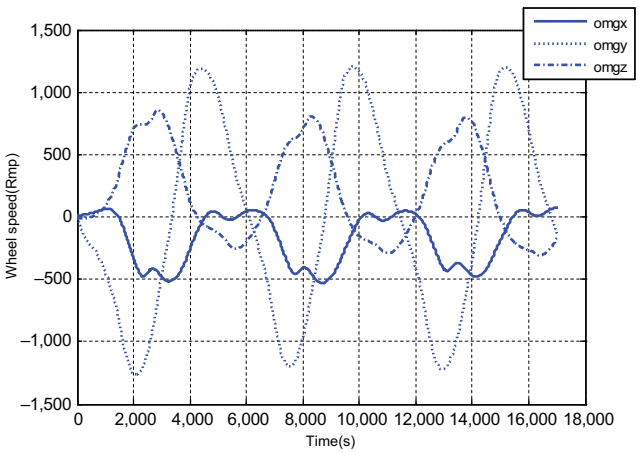

Figures 9 and 10 show that the maximum wheel speed decreases when a magnetic unloading control is executed. The maximum wheel speed of Figure 9 is 2,800 rpm, and the maximum wheel speed of Figure 10 is 1,200 rpm, which show that the proposed magnetic unloading algorithm is valid.

Figure 11 Time histories of Euler angle

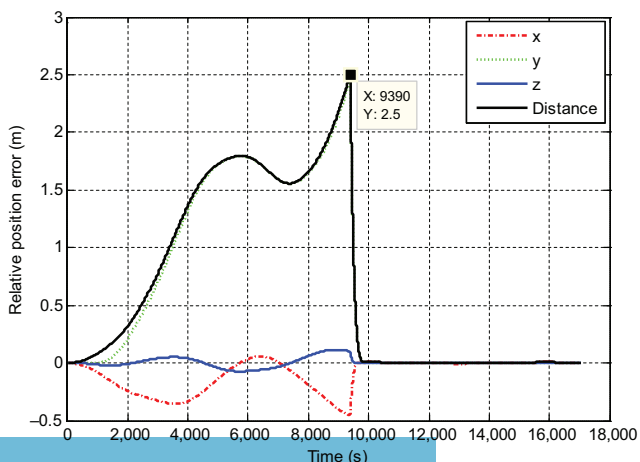

Figure 12 Enlarged view of Figure 11

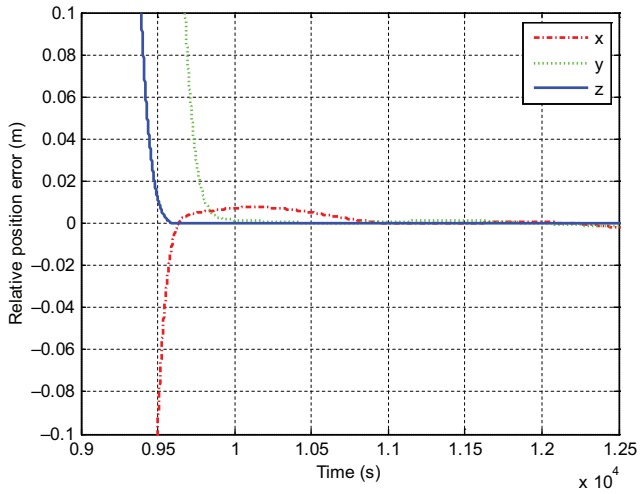

Figure 13 Time histories of sliding mode manifold

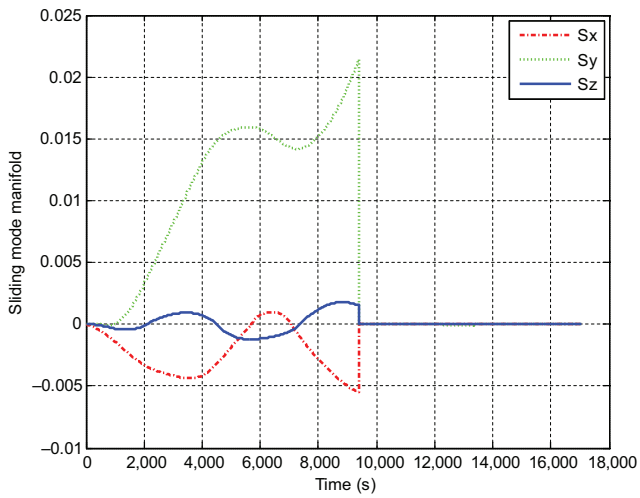

Figure 14 Time histories of the earth's magnetic field of the reference orbit

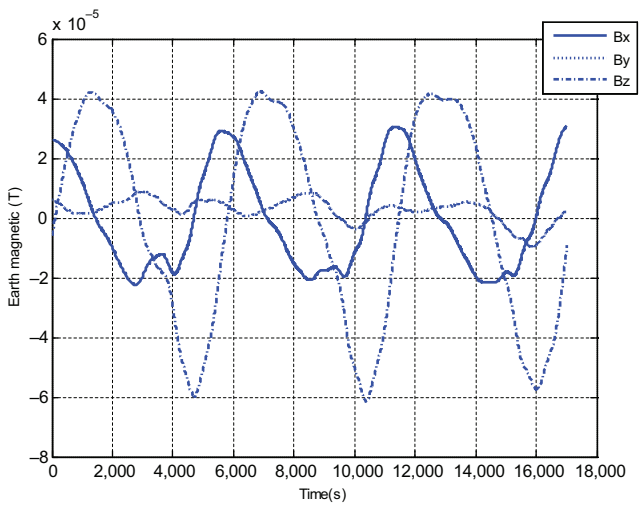

Scenario 3. Two satellite formation-keeping scenario. A two-satellite EMFF-keeping scenario is carried out to verify the terminal sliding mode controller as described in equation (60). The reference orbit parameters are the same as those described in Scenario 1, and the formation configuration is chosen as $\{p = 15$ m, $s = 20$, $\alpha = 0°$, $\theta = 0°$, $l = 0\}$ (Zeng *et al.*, 2012a, 2012b). Once the formation configuration is pertubated over 10 per cent of the nominal formation geometry, the terminal sliding mode controller is activated. The coil radius is 1 m and the mass for each coil is 20 kg, and the maximum magnetic moment is $1.625e^5$ Am^2. The control parameters are listed as $\alpha = [0.01, 0.01, 0.01]^T$, $\beta = [0.01, 0.01, 0.01]^T$, $\gamma = 0.8$, $k = [0.96, 0.96, 0.96]^T$ and $\phi = 1$.

Figure 15 Variations of magnetic force

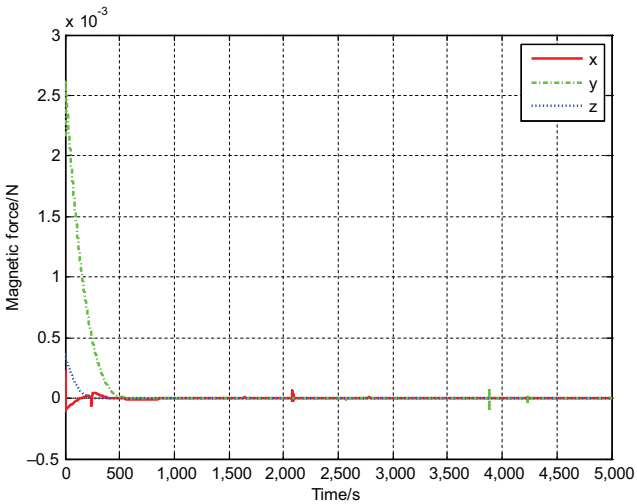

Figure 11 shows the time histories of the relative position error, Figure 12 is the enlarged version of Figure 11 and Figure 13 shows the time histories of the sliding mode manifold.

In Figure 11, the terminal sliding mode controller activated at the time t = 9,390 s, when the relative distance error reaches the predefined threshold of 2.5 m.

The International Geomagnetic Reference Field (IGRF) model is adopted to describe the earth's main magnetic field. The variations of the earth's magnetic field of the reference orbit are shown in Figure 14.

As shown in Figure 14, the maximum magnitude of the earth's magnetic field of the reference orbit is 6.082e–5 T. Figure 15 plots the magnetic force variations once the actuators are executed.

Figure 16 shows the control allocation of magnetic control moment of sat_1 and sat_2.

From Figure 16, we can see that the variation law of allocation results are consistent with those of the magnetic force.

Conclusion

This paper presents the attitude and relative translation control law for EMFF satellites in low earth orbit. First, the attitude and relative translational dynamics equations are derived. Then, the feedback attitude control law, the unloading algorithm of reaction wheels and the large angle manoeuvre algorithm are presented. The terminal sliding mode controller for relative translational motion is also put forward. The control allocation problem is formulated as an optimization issue and a hybrid particle swarm optimization (PSO) – sequential quadratic programming (SQP) algorithm is used to calculate the free dipole. Finally, numerical simulations are performed to validate

Figure 16 Allocation results of magnetic moments

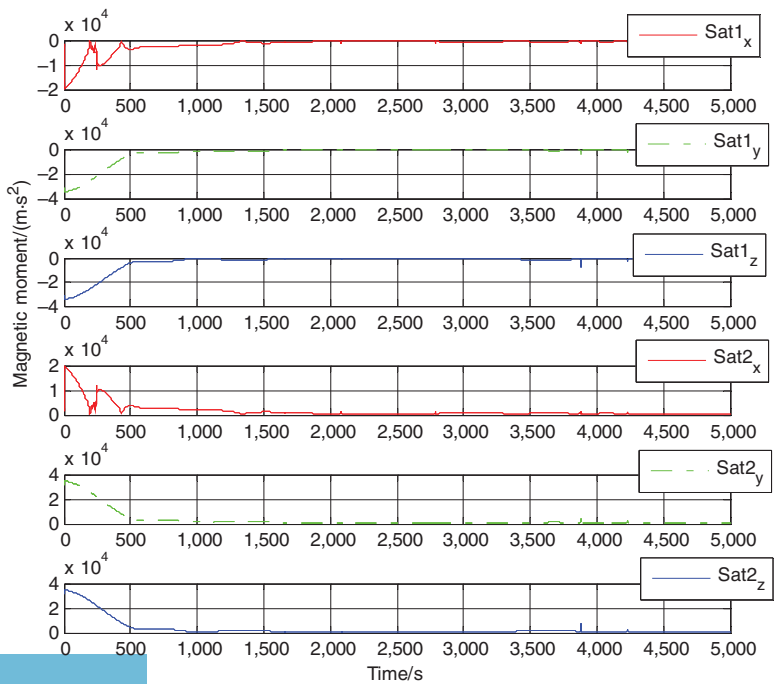

the proposed controller. The sun-tracking scenario, magnetic unloading scenario and formation-keeping scenario show that the proposed controllers are effective and can be implemented for future EMFF missions.

References

Ahsun, U., Miller, D.W. and Ramirez, J.L. (2010), "Control of electromagnetic satellite formations in near-Earth orbits", *Journal of Guidance, Control, and Dynamics*, Vol. 33 No. 6, pp. 1883-1891.

Alvisio, B. (2015), *Development and Validation of An Electromagnetic Formation Flight Simulation As A Platform for Control Algorithm Design*, Institute of Technology, Massachusetts.

Cai, W.W., Yang, L.P., Zhu, Y.W. and Zhang, Y.W. (2013), "Formation keeping control through inter-satellite electromagnetic force", *Science China Technological Sciences*, Vol. 56 No. 5, pp. 1102-1111.

Chak, Y.C. and Varatharajoo, R. (2015), "A novel design of spacecraft combined attitude & sun tracking system using a versatile fuzzy controller", *Aircraft Engineering and Aerospace Technology: An International Journal*, Vol. 87 No. 6, pp. 530-539.

Ding, S.H. and Li, S.H. (2007), "Finite time tracking control of spacecraft attitude", *Acta Aeronautica et Astronautica Sinica*, Vol. 28 No. 3, pp. 628-633.

Huang, X.L., Zhang, C. and Ban, X.J. (2016), "Dipole solution and angular-momentum minimization for two-satellite electromagnetic formation flight", *Acta Astronautica*, Vol. 119 Nos 2/3, pp. 79-86.

Huang, X.L., Zhang, C., Lu, H.Q. and Yin, H. (2015), "An LMI-based decoupling control for electromagnetic formation flight", *China Journal of Aeronautics*, Vol. 28 No. 1, pp. 508-517.

Ismail, Z., Varatharajoo, R., Ajir, R. and Rafie, A. (2015), "Enhanced attitude control structure for small satellites with reaction wheels", *Aircraft Engineering and Aerospace Technology: An International Journal*, Vol. 87 No. 6, pp. 546-550.

Kennedy, J. and Eberhart, R. (1995), "Particle swarm optimization", *Proceedings of the IEEE International Conference on Neural Network, Perth*, pp. 1942-1948.

Kong, E.M.C., Kwon, D.W., Schweighart, S.A., Elias, L.M., Sedwick, R.J. and Miller, D.W. (2004), "Electromagnetic formation flight for multisatellite arrays", *Journal of Spacecraft and Rockets*, Vol. 41 No. 4, pp. 659-666.

Liu, H. and Li, J.F. (2009), "Terminal sliding mode control for spacecraft formation flying", *IEEE Transactions on Aerospace and Electronic Systems*, Vol. 45 No. 3, pp. 835-846.

Porter, A.K., Alinger, D.J. and Sedwick, R.J. (2014), "Demonstration of electromagnetic formation flight and wireless power transfer", *Journal of Spacecraft and Rockets*, Vol. 51 No. 6, pp. 1914-1923.

Schweighart, S.A. (2005), *Electromagnetic Formation Flight Dipole Solution Planning*, Massachusetts Institute of Technology, Massachusetts.

Wilson, R.B. (1963), *A Simplicial Algorithm for Concave Programming*, Graduate School of Business Administration, Harvard University, Boston.

Wu, S.N., Radice, G., Gao, Y.S. and Sun, Z.W. (2011), "Quaternion-based finite time control for spacecraft attitude tracking", *Acta Astronautica*, Vol. 69 Nos 1/2, pp. 48-58.

Wu, S.N., Wang, R., Radice, G. and Wu, Z.G. (2015), "Robust attitude maneuver control of spacecraft with reaction wheel low-speed friction compensation", *Aerospace Science and Technology*, Vol. 43, pp. 213-218.

Yu, X., Wu, Y. and Man, Z. (1999), "Variable structure systems with terminal sliding modes", *Acta Astronautica*, Vol. 119, pp. 79-86, Variable structure systems: towards the 21st Century, Lecture notes in control and information sciences, Springer, Vol. 274, pp. 109-122.

Zeng, G.Q. and Hu, M. (2012), "Finite-time control for electromagnetic satellite formations", *Acta Astronautica*, Vol. 74 No. 1, pp. 120-130.

Zeng, G.Q., Hu, M. and Song, J.L. (2012a), "Collision monitoring and optimal collision avoidance manoeuvre for formation flying satellites", *Aircraft Engineering and Aerospace Technology: An International Journal*, Vol. 84 No. 6, pp. 413-422.

Zeng, G.Q., Hu, M. and Yao, H. (2012b), "Relative orbit estimation and formation keeping control of satellite formations in low Earth orbits", *Acta Astronautica*, Vol. 76 No. 1, pp. 164-175.

Zhang, J.R., Yuan, C.Q., Jiang, D.M. and Jin, D.W. (2014), "Adaptive terminal sliding mode control of electromagnetic spacecraft formation flying in near-Earth orbits", *Advances in Mechanical Engineering*, Vol. 2014 No. 1, pp. 1-9.

Corresponding author

Min Hu can be contacted at: songjl@mail.ustc.edu.cn